


Limitations of the equivalent neutral polymer assumption for theories describing nanochannel-confined DNA

Aditya Bikram Bhandari and Kevin D. Dorfman ^{*}

*Department of Chemical Engineering and Materials Science, University of Minnesota,
Twin Cities, 421 Washington Ave. SE, Minneapolis, Minnesota 55455, USA*



(Received 31 October 2019; published 13 January 2020)

The prevailing theories describing DNA confinement in a nanochannel are predicated on the assumption that wall-DNA electrostatic interactions are sufficiently short-ranged such that the problem can be mapped to an equivalent neutral polymer confined by hard walls with an appropriately reduced effective channel size. To determine when this hypothesis is valid, we leveraged a recently reported experimental data set for the fractional extension of DNA molecules in a 250-nm-wide poly(dimethyl siloxane) (PDMS) nanochannel with buffer ionic strengths between 0.075 and 48 mM. Evaluating these data in the context of the weakly correlated telegraph model of DNA confinement reveals that, at ionic strengths greater than 0.3 mM, the average fractional extension of the DNA molecules agree with theoretical predictions with a mean absolute error of 0.04. In contrast, experiments at ionic strengths below 0.3 mM produce average fractional extensions that are systematically smaller than the theoretical predictions with a larger mean absolute error of 0.15. The deviations between experiment and theory display a correlation coefficient of 0.82 with the decay length for the DNA-wall electrostatics, linking the deviations with a breakdown in approximating the DNA with an equivalent neutral polymer.

DOI: [10.1103/PhysRevE.101.012501](https://doi.org/10.1103/PhysRevE.101.012501)

I. INTRODUCTION

DNA in channel confinement stretches out from its coiled structure in free solution [1] to a significant fraction of its contour length, and exhibits a rich variety of confinement regimes [2–4]. Theories developed over the past decade have described semiflexible polymers in weak confinement where the polymer still has a locally coiled blob structure [2,5–17], moderate confinement characterized by occasional hairpins in the polymer backbone [16–26], and strong confinement where the polymer is stretched to a significant fraction of its contour length [17,27–29]. The fractional extension realized in confinement depends on the DNA stiffness, the extent of segmental excluded volume, and the size of the confining channel. Although DNA is a polyelectrolyte and the confining channels typically are fabricated from materials that possess surface charges, theories describing the fractional extension [2] simplify the problem to that of a neutral semiflexible chain confined by hard channel walls, using conventional polyelectrolyte theory to account for electrostatic effects on the DNA persistence length [30] and excluded volume [31,32]. The electrostatic interactions also appear as a wall-DNA depletion length [3,33,34] that yields a reduced effective channel size for use in the theoretical models.

Remarkably, these simplified “neutral polymer” models are able to describe to a great extent previous experimental observations of DNA in nanochannel confinement despite their neglect of the details of the electrostatic interactions [16,35].

In particular, there is a relatively large body of experimental work on channel-confined DNA using large nanochannels and high ionic strengths [36–41], corresponding to weak confinement conditions, for which the wall-DNA depletion length is negligible compared to the channel dimensions. However, experiments probing strong confinement used either sub-50-nm channels at high ionic strengths [34,42,43] or low ionic strengths in relatively large channels [18,37,44]. Long-range electrostatic effects become much more pronounced for experiments with a decrease in channel size and/or ionic strength, owing to an increased magnitude of the Debye length relative to the channel size.

To properly quantify the effect of electrostatics on the agreement between theory and experiment, it is illuminating to compare experimental observations under varying degrees of confinement to a theory spanning multiple confinement regimes. The recently proposed telegraph model [16] provides such a tool. This model treats the problem of DNA stretching as a one-dimensional random walk, furnishing master curves for the fractional extension as a function of a single scaling parameter α , which denotes the number of overlaps per hairpin bend in the DNA. The average fractional extension predicted by the telegraph model agrees with pruned-enriched Rosenbluth method (PERM) simulations [33,45] for a confined semiflexible polymer, and the asymptotic predictions for the distributions of the fractional extension [26] are robust even under simulation conditions which do not strictly satisfy the asymptotic conditions in the theory [46].

Experiments involving confined DNA, although agreeing with the general trends predicted by the telegraph model [16,26], exhibit obvious quantitative discrepancies.

^{*}dorfman@umn.edu.

The observed average fractional extension values are generally overpredicted by the theory [16], and the deviations between experiment and theory become more apparent when comparing theory and experimental data for the fractional extension distributions [26,47]. A possible explanation for these discrepancies, in particular those in the fractional extension distributions [26,47] obtained in sub-50-nm channels, is that the lengthscale for the decay of electrostatic effects becomes comparable to the channel size for small channel sizes [47] or low ionic strengths. However, the point at which the DNA-wall electrostatic interactions begin to affect the agreement between theory and experiment remains an open question.

An overarching problem in addressing the impact of DNA-wall electrostatic interactions is that prior experiments involving confined DNA tended to focus on specific confinement regimes, thus making their collective comparison to theory susceptible to inhomogeneity in operating conditions. A recent data set generated by Lee *et al.* [48] helps overcome this limitation. Their experiments used DNA stained with TAMRA-polypyrrole in 250-nm channels with varying ionic strengths from typical high ionic strength buffers down to very weak buffers. While Lee *et al.* [48] made a comprehensive study of the effect the new staining agent has on DNA visualization and a preliminary scaling analysis, a quantitative examination of the data in the context of the state-of-the-art theories is an unexplored avenue. In this study, we leveraged their data set to test the telegraph theory [16] over several decades in its scaling parameter within a single experimental protocol, thereby illuminating the point at which the neutral polymer assumption breaks down.

II. THEORY AND METHODS

Comparison between experiment and theory requires computing four system parameters: the DNA contour length L , persistence length l_p , effective width w , and the effective channel size D_{eff} . The experiments by Lee *et al.* [48] used T4 GT7 (166 kilobase pair, kbp) DNA stained with TAMRA-polypyrrole confined in square poly(dimethyl siloxane) (PDMS) nanochannels with a channel size of $D = 250$ nm and ionic strengths ranging from extremely low values of $I = 0.07$ mM to a more conventional value [34,43] of $I = 47$ mM. The dye is not expected to affect the contour length [48], whereupon the estimate for the contour length is $L = 55.8 \mu\text{m}$. The remaining polymer parameters, which are a function of the ionic strength I , include the persistence length l_p , which denotes the DNA stiffness [30]

$$l_p[\text{nm}] = 46.1 + \frac{1.9195}{\sqrt{I[\text{M}]}} \quad (1)$$

and the DNA effective width w [31,32], which is indicative of the excluded volume between DNA segments

$$w = \lambda_D \left[0.7704 + \log \left(\frac{\nu_{\text{eff}}^2 \lambda_D}{2\epsilon\epsilon_0 k_B T} \right) \right]. \quad (2)$$

In the latter, λ_D is the Debye length, ϵ is the dielectric constant of the buffer, ϵ_0 is the permittivity of free space, and $k_B T$ is the Boltzmann factor. The term ν_{eff} is the effective charge density of DNA as described by Stigter [31].

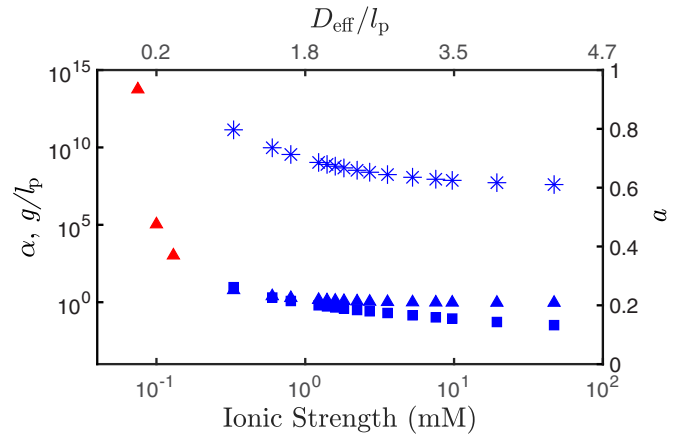


FIG. 1. Dependence of the telegraph model parameters on ionic strength and the corresponding ratio of D_{eff}/l_p : α (squares), denoting the number of overlaps per hairpin in the DNA backbone; the global persistence length g (triangles) denoting the typical distance between hairpin bends; and the alignment factor a (asterisks) denoting the average alignment between the DNA backbone and the axis of the channel. The blue data were interpolated from the simulation data by Werner *et al.* [16]. The red data correspond to the three lowest ionic strengths, which fall outside the range considered by Werner *et al.* [16]. We have not reported the parameters a and α for these ionic strengths as they do not follow the telegraph model. The calculations of the global persistence length for the red data use the model of Eq. (4) [20].

Experiments indicate that the wall-DNA depletion length δ [34] scales linearly with the Debye length as

$$\delta[\text{nm}] = 6.5\lambda_D[\text{nm}] - 0.64. \quad (3)$$

This depletion length is converted to an effective channel size via $D_{\text{eff}} = D - \delta$. The parameters are tabulated in Table S-1 of the Supplemental Material [49] for each of the ionic strengths used in the experiments [48]. The resulting range of D_{eff} was between 20 to 241 nm, and the average fractional extensions ranged from $X/L = 0.85$ to $X/L = 0.22$.

The weakly correlated telegraph model [16], which we will use for the most part to compare theory with the experimental results, maps the confined DNA problem to a problem of a one-dimensional random walk. The velocity of the walk corresponds to the average alignment of the polymer backbone with the channel axis a . The walk changes direction at a rate $r = 1/(2g)$, where g is the global persistence length, quantifying the average distance between hairpins in the DNA backbone. The penalty parameter ϵ accounts for the effect of self-avoidance. The scaling parameter for the telegraph model α is obtained from dimensional analysis as $\alpha = \epsilon g/a$. When possible, the telegraph model parameters are obtained via interpolation of the data computed by Werner *et al.* [16]. The blue data points in Fig. 1 illustrate how these parameters vary with ionic strength for $D = 250$ nm in the range $0.4 < D_{\text{eff}}/l_p < 24$, the region for which Werner *et al.* [16] obtained simulation data.

The three data points colored red correspond to g , for the lowest ionic strengths. The concomitant channel sizes $D_{\text{eff}}/l_p < 0.4$ and are outside the range for interpolation from

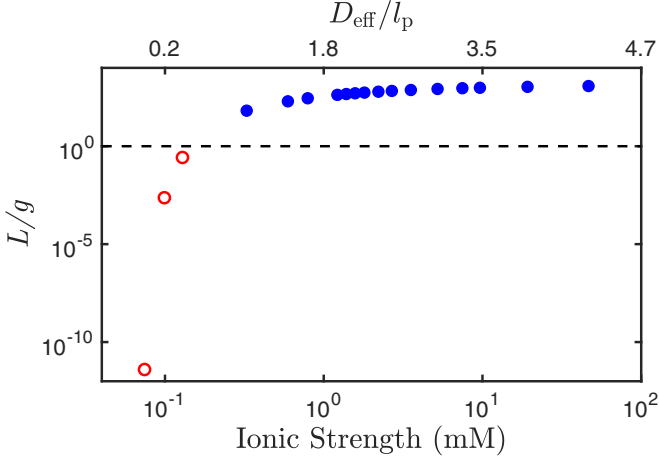


FIG. 2. The ratio of the DNA contour length L to the global persistence length g as a function of the ionic strength and the corresponding ratio of D_{eff}/l_p . The dashed line indicates the point $L = g$, where the chain is long enough to form a hairpin in the channel. Only the solid blue circles satisfy the hairpin formation criterion for the telegraph model.

Werner *et al.* [16]. Rather than extrapolate the data from Werner *et al.* [16], we instead obtained g from the modification of Odijk's global persistence length theory [50] by Muralidhar *et al.* [20]. The global persistence length in this model is given by

$$g = f\bar{r} \exp\left(\frac{\bar{F}_{\text{mc}}}{k_{\text{B}}T} - 4.91\right), \quad (4)$$

where $f = 3.3082$ is a constant [50] and \bar{r} is the average length of a hairpin chord

$$\bar{r} = \frac{l_p}{6} \left[\left[E_m^2 + 6\sqrt{2}E_m \left(\frac{D_{\text{eff}}}{l_p} \right) \right]^{1/2} - E_m \right], \quad (5)$$

where $E_m = 1.5071$ is another constant [50]. The mechanical contribution to the free energy \bar{F}_{mc} in Eq. (4) is

$$\frac{\bar{F}_{\text{mc}}}{k_{\text{B}}T} = E_m \left(\frac{l_p}{\bar{r}} \right) - 3 \ln \left(\frac{D_{\text{eff}} - \sqrt{2}\bar{r}}{D_{\text{eff}}} \right) - \ln \left(\frac{8}{3\pi} \right), \quad (6)$$

Note that Chen [51] identified errors in Odijk's derivation for circular channels [50]. However, since the simulation data of Muralidhar *et al.* [22] for circular channels is in good agreement with Chen's theory [51], it is reasonable to continue to use Eq. (4) for rectangular channels since it is also in good agreement with the simulation data of Muralidhar *et al.* [20] for square channels.

Figure 2 plots the number of global persistence lengths L/g as a function of ionic strength for the data set from Lee *et al.* [48]. Interestingly, the situations for $D_{\text{eff}}/l_p > 0.4$, where we were able to interpolate the telegraph parameters from Werner *et al.* [16] in Fig. 1, also correspond to $L > g$, where we would expect the telegraph model predictions to be reasonably accurate. In these cases, we then interpolate the average fractional extension obtained by Werner *et al.* [16] to compare to the experimental data. In contrast, the red open circles in Fig. 2, which correspond to the lowest ionic

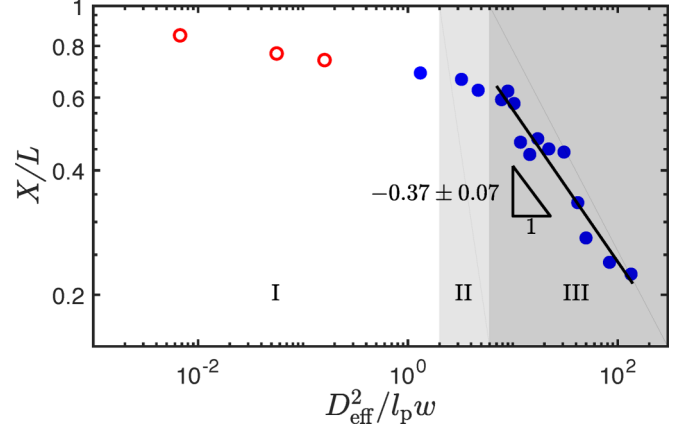


FIG. 3. Average fractional extension X/L from the experimental data in Lee *et al.* [48] plotted against the blob regime scaling variable $D_{\text{eff}}^2/l_p w$. The red (open circles) and blue (closed circles) coding follows from Fig. 2. The increasing shading corresponds to regimes of strong confinement (I), a “transition” regime (II) and a weak confinement regime (III). The data in regime III scale with an exponent of -0.37 , in agreement with the slightly different analysis of Lee *et al.* [48].

strengths, are conditions of very strong confinement (due to the increase in l_p and δ as ionic strength increases), but using chains that are much too short to form a hairpin. For these cases, the telegraph model is clearly not valid. For this reason, we did not attempt to extrapolate values of a and α for these ionic strengths from the data of Werner *et al.* [16] in Fig. 1. We instead use the Odijk theory [27]

$$\frac{X_{\text{Odijk}}}{L} = 1 - 0.18274 \left(\frac{D_{\text{eff}}}{l_p} \right)^{2/3}, \quad (7)$$

with the numerical prefactor obtained by Burkhardt *et al.* [29].

For completeness, all of the relevant parameters are tabulated in the Supplemental Material [49] as a function of the ionic strength.

III. RESULTS AND DISCUSSION

We first present the experimental data of Lee *et al.* [48] in a manner similar to their analysis: the unshaded region (I), light gray shaded region (II), and the dark gray shaded region (III) in Fig. 3 correspond to the strong confinement regime, the “transition” regime, and the weak confinement regime, respectively. The data points are colored red (open circles) or blue (closed circles) depending on the applicability of the telegraph model, as detailed in Sec. II.

In our analysis, we computed the persistence length using Dobrynin's theory [30] in Eq. (1) rather than the modified result of Lee *et al.* [48]

$$l_p[\text{nm}] = 42.1 + \frac{1.90}{\sqrt{I[\text{M}]}}. \quad (8)$$

Nevertheless, we obtained the same slope of -0.37 ± 0.07 for the data points in region III. The uncertainty reported here and hereafter refers to the 95% confidence interval. The similarity

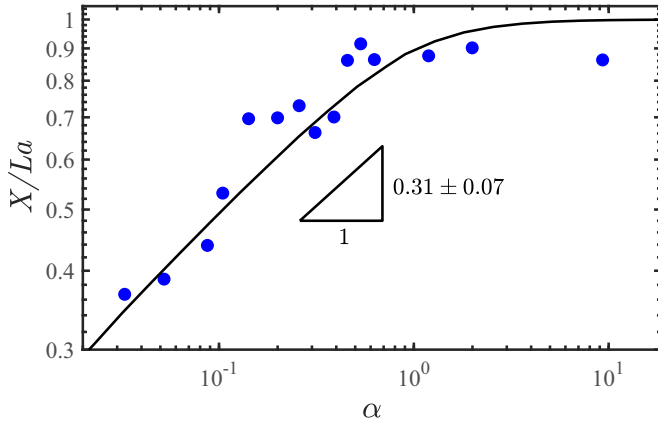


FIG. 4. Average fractional extension X/L from the experimental data in Lee *et al.* [48] that satisfy the conditions for the telegraph model (blue circles) and the numerical simulation of the telegraph model (solid black line) [16]. The data in the scaling region of the telegraph model for $\alpha \ll 1$ display a scaling exponent of 0.31 ± 0.07 , which contains the theoretical value of the exponent, $1/3$, in its 95% confidence interval.

between the scaling exponent obtained using Eq. (1) versus Eq. (8) arises because these two equations exhibit only small differences for the relatively high ionic strengths used in the weak confinement regime.

We also considered the effects of measurement error in the dependent variable X/L as well as the independent variable $D_{\text{eff}}^2/l_p w$, by propagating the uncertainty in the channel size and ionic strength. Since this second analysis considers uncertainty in both the dependent and independent variables, we performed an errors in variables regression method known as Deming regression, which takes into account the error in both the independent and dependent coordinates. This regression method led to no statistically significant change in the slope, -0.37 ± 0.06 , when compared to regression that only considers the uncertainty in the dependent variable [48]. Details of the error propagation and Deming regression are provided in the Supplemental Material [49].

Figure 4 now analyzes the blue solid circles in Fig. 3 in the context of the telegraph model. The red open circles in Fig. 3, which do not satisfy the condition $L \gg g$, are excluded from this analysis. The telegraph model predicts that regime III of Fig. 3 scales as $X/La \sim \alpha^{1/3}$. Linear regression of the experimental data, corresponding to regime III of Fig. 3 on a log-log scale, yields a slope of 0.31 ± 0.07 , which is in agreement with the theoretical value to within a 95% confidence interval. Deming regression, accounting for the errors in the experimentally observed values of fractional extension and in α by propagation of errors in the ionic strength and channel size, yielded only a slight difference in the slope, 0.31 ± 0.06 , which was not statistically significant.

For regions I and II of Fig. 3, which include the red open circles that do not satisfy the conditions for the telegraph model, we compared the experimental data to the predictions of the fractional extensions in the Odijk regime in Eq. (7). Figure 5 plots the average fractional extension against the relevant scaling parameter for the Odijk regime D_{eff}/l_p . Taken together, Figs. 4 and 5 reveal that, while the blue (solid

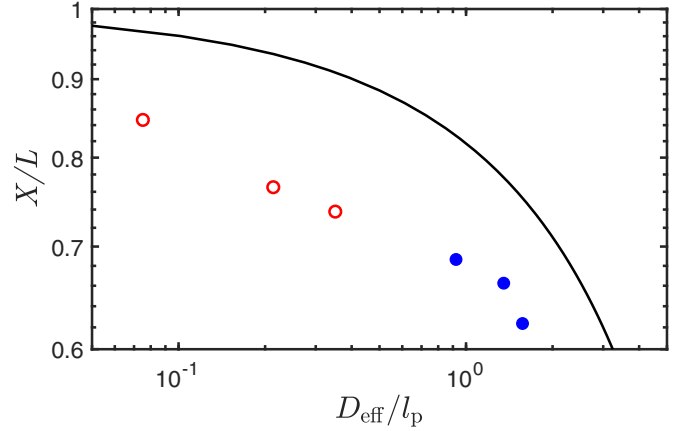


FIG. 5. Average fractional extension X/L from the experimental data in Lee *et al.* [48] in regions I and II of Fig. 3, including the data points which do not satisfy the conditions for the telegraph model (red open circles), and the corresponding theoretical predictions from the Odijk theory (solid black line) plotted against the relevant scaling parameter in the Odijk regime D_{eff}/l_p .

circle) fractional extension data that satisfy the assumptions for telegraph model exhibit a mean absolute error (MAE) of 0.04 between the theory and experiment, there is a substantial increase in the average deviation to an MAE of 0.15 for the red open circles, which correspond to lower ionic strengths. Moreover, Fig. 5 exhibits a systematic deviation between theory and experiment, while Fig. 4 furnishes a deviation between theory and experiment that might be expected due to random errors.

Chuang *et al.* [47] recently identified a possible shortcoming in the models describing the stretching of confined DNA because they neglected the effect of DNA-wall electrostatics. We probed the possibility that this effect may be amplified for the lower ionic strengths. While simply computing the Debye length [52] may provide a useful proxy for understanding the impact of DNA-wall electrostatic interactions, it is illustrative to calculate the cutoff length for the decay of electrostatics z^* as a fraction of the channel size D by following the calculations of Chuang *et al.* [47].

Briefly, the wormlike chain propagator $q(\mathbf{r}, \mathbf{u}; t)$ in the presence of an external potential field is [17]

$$\frac{\partial}{\partial t} q(\mathbf{r}, \mathbf{u}; t) = \left[-\mathbf{u} \cdot \nabla_{\mathbf{r}} + \frac{1}{2} \nabla_{\mathbf{u}}^2 - \beta \phi(\mathbf{r}, \mathbf{u}) \right], \quad (9)$$

where \mathbf{r} , \mathbf{u} , and t are the dimensionless position vector, tangent vector, and position along the contour length, respectively, and $\beta \phi(\mathbf{r}, \mathbf{u})$ accounts for the polymer-wall electrostatic interactions. The parameter β is the characteristic polymer-wall interaction energy per deflection segment

$$\beta = \frac{U(z=0) \lambda}{k_B T L}, \quad (10)$$

where $\lambda = (l_p D_{\text{eff}}^2)^{1/3}$ is the Odijk deflection length [27] and $U(z) = v_{\text{eff}} \psi_{\text{wall}} e^{-z/\lambda_D} L$ is the polymer-wall interaction energy for a polymer segment of effective charge density v_{eff} in a medium with a Debye length of λ_D due to the potential $\psi(z) = \psi_{\text{wall}} e^{-z/\lambda_D}$ [3]. Note that this definition of

β does not depend on the stretching regime, as the possible contributions of other effects such as excluded volume under weak confinement add additional terms to Eq. (9) but do not affect the nondimensionalization of the electrostatics term in Eq. (9). We consider the effect of electrostatics to be negligible when the term $\beta\phi = 0.1$, which occurs at some cutoff value for the decay length z^* .

Within this simple model for the polymer-wall interactions, the wall potential [3] is

$$\psi_{\text{wall}} = \frac{4k_B T}{e} \tanh\left(\frac{e\zeta}{4k_B T}\right), \quad (11)$$

where e is the elementary charge of an electron. This calculation in turn requires a zeta potential ζ , which we obtained from Behren and Grier's model [53] by simultaneously solving

$$\zeta(\sigma) = \frac{k_B T}{e} \log\left(\frac{-\sigma}{e\Gamma + \sigma}\right) - (\text{pH} - \text{pK}) \frac{k_B T \log(10)}{e} - \frac{\sigma}{C} \quad (12)$$

and

$$\sigma(\zeta) = \frac{2\epsilon\epsilon_0 k_B T}{e\lambda_D} \sinh\left(\frac{e\zeta}{2k_B T}\right), \quad (13)$$

where σ is the surface charge density, $\epsilon_0 = 8.85 \times 10^{-12}$ F/m is the permittivity of free space, and ϵ is the dielectric constant. We assumed the well-characterized properties of glass for simplicity (chargeable site density $\Gamma = 8 \text{ nm}^{-2}$, Stern layer capacity $C = 2.9 \text{ F/m}^2$) and assumed a pH of 8.6 [34] and a dissociation constant of $\text{pK} = 7.5$. The values of ψ_{wall} calculated in this manner range from -77 to -96 mV and are indeed larger than the small potentials for which the Poisson Boltzmann theory may be linearized to give the Debye-Hückel theory in Eq. (11) [54]. However, the full solution to the Poisson Boltzmann equation decays at a rate faster than that of Eq. (11) [55], thus making our estimate of z^* a conservative one.

Note that the PDMS channels used in the experiments have a zeta potential typically larger than glass [56,57]. This increases the wall potential ψ_{wall} , and hence β , thus requiring a lower value of ϕ and a larger value of z^* to satisfy the decay condition $\beta\phi = 0.1$. This implies that corrections for PDMS channels would only serve to increase the decay length, thus strengthening the evidence for any correlation between electrostatics and the deviations.

Figure 6 reveals that this cutoff length correlates positively with the deviation between experiment and theory for these experiments. The correlation coefficient is 0.82 and is statistically significant, with a p-value of 2×10^{-5} . Thus, the equivalent neutral polymer assumption is found to indeed be limited by the effect of long-range electrostatics in the system.

IV. CONCLUSION

We exploited the experimental dataset by Lee *et al.* [48], which spans multiple regimes of DNA confinement, to discern when the effect of long-range electrostatics in the system can no longer be neglected and the equivalent neutral polymer assumption breaks down. We found that the data exhibiting

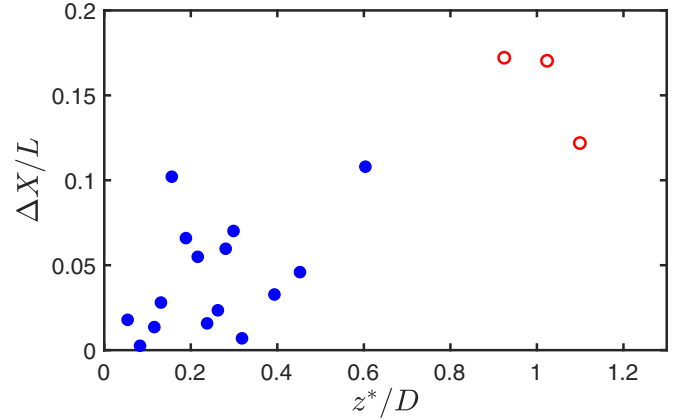


FIG. 6. The deviation of the fractional extension $\Delta X/L$ versus the cutoff value of the normalized decay length z^*/D . The deviation is defined as the absolute value of the difference between the experimentally observed average fractional extension and the theoretical prediction for the same parameters. The decay length cutoff is defined as the point at which $\beta\phi = 0.1$. The correlation coefficient between these variables is 0.82.

modest confinement and satisfying the assumptions for the telegraph model [16] agree well with experiment. However, for stronger confinement, and particularly for the Odijk regime, there is a significant deviation between theory and experiment. Our observations are consistent with the findings of Chuang *et al.* [47], who reported a significant effect of long-range electrostatics for DNA confined in sub-50-nm channels. There exists a positive correlation between the decay length of the electrostatics and the deviation between experiment and theory, thus suggesting that the breakdown between theory and experiment is consistent with the emerging importance of DNA-wall electrostatic interactions.

Even though these experiments provide significant insights into the nature of the discrepancies between experiment and theory, there are some factors confounding the analysis. First, these experiments were performed using PDMS nanochannels, which are porous at a molecular scale and facilitate alterations of the buffer condition [58–60]. One notable possibility is the absorption of carbon dioxide by the buffer from the atmosphere (a well-known potential problem for low ionic strength buffers [61]). Such absorption would decrease the pH of the solution, causing a decrease in the negative wall potential of the PDMS nanochannel [56]. The change in wall potential would, in turn, cause less repulsion between the DNA and the channel wall, hence decreasing the fractional extension. A possible resolution to the problem is performing similar experiments in fused silica nanochannels, which would limit carbon dioxide transport. In the absence of a less porous nanochannel material, it is worthwhile to evaluate the effect of carbon dioxide absorption into the buffer by measuring the average fractional extension of the DNA molecules at different points in time, with the hypothesis that the increasing acidity will cause a systematic reduction in the stretching with time. Second, the assumption of a linear model for the DNA-wall depletion length [34] breaks down for ionic strengths less than 5 mM, thus causing added uncertainty to our analysis of the low ionic strength results. These factors

suggest that the discrepancies between experiment and theory at low ionic strengths might be slightly exaggerated. We anticipate that this study will motivate more directed experiments in the future to compare experiment and theory, as well as a thorough re-evaluation of the treatment of electrostatics in the prevailing theories.

ACKNOWLEDGMENTS

We thank Seonghyun Lee and Prof. Kyubong Jo of Sogang University, South Korea, for providing us with the raw data for their paper [48]. This work was supported by the National Institutes of Health (Grant No. NIH R01-HG006851).

- [1] M. Doi and S. F. Edwards, *The Theory of Polymer Dynamics*, Vol. 73 (Oxford University Press, New York, 1988).
- [2] T. Odijk, *Phys. Rev. E* **77**, 060901(R) (2008).
- [3] W. Reisner, J. N. Pedersen, and R. H. Austin, *Rep. Prog. Phys.* **75**, 106601 (2012).
- [4] L. Dai, C. B. Renner, and P. S. Doyle, *Adv Colloid Interface Sci.* **232**, 80 (2016).
- [5] M. Daoud and P. G. de Gennes, *J. Phys.* **38**, 85 (1977).
- [6] P.-G. De Gennes, *Scaling Concepts in Polymer Physics* (Cornell University Press, Ithaca, NY, 1979).
- [7] Y. Jung, S. Jun, and B.-Y. Ha, *Phys. Rev. E* **79**, 061912 (2009).
- [8] D. R. Tree, Y. Wang, and K. D. Dorfman, *Phys. Rev. Lett.* **110**, 208103 (2013).
- [9] E. Werner and B. Mehlig, *Phys. Rev. E* **90**, 062602 (2014).
- [10] L. Dai and P. S. Doyle, *Macromolecules* **46**, 6336 (2013).
- [11] J. Kim, C. Jeon, H. Jeong, Y. Jung, and B.-Y. Ha, *Soft Matter* **9**, 6142 (2013).
- [12] Y.-L. Chen, *Biomicrofluidics* **7**, 054119 (2013).
- [13] J. Z. Y. Chen, *Macromolecules* **46**, 9837 (2013).
- [14] L. Dai, J. R. C. van der Maarel, and P. S. Doyle, *Macromolecules* **47**, 2445 (2014).
- [15] E. Werner and B. Mehlig, *Phys. Rev. E* **91**, 050601(R) (2015).
- [16] E. Werner, G. K. Cheong, D. Gupta, K. D. Dorfman, and B. Mehlig, *Phys. Rev. Lett.* **119**, 268102 (2017).
- [17] J. Z. Y. Chen, *Phys. Rev. Lett.* **121**, 037801 (2018).
- [18] C. Zhang, F. Zhang, J. A. van Kan, and J. R. C. van der Maarel, *J. Chem. Phys.* **128**, 225109 (2008).
- [19] L. Dai, S. Y. Ng, P. S. Doyle, and J. R. van der Maarel, *ACS Macro Lett.* **1**, 1046 (2012).
- [20] A. Muralidhar, D. R. Tree, and K. D. Dorfman, *Macromolecules* **47**, 8446 (2014).
- [21] A. Muralidhar, M. J. Quevillon, and K. D. Dorfman, *Polymers* **8**, 79 (2016).
- [22] A. Muralidhar and K. D. Dorfman, *Macromolecules* **49**, 1120 (2016).
- [23] E. Werner, A. Jain, A. Muralidhar, K. Frykholm, T. St Clere Smithe, J. Fritzsche, F. Westerlund, K. Dorfman, and B. Mehlig, *Biomicrofluidics* **12**, 024105 (2018).
- [24] J. Krog, M. Alizadehheidari, E. Werner, S. K. Bikkarolla, J. O. Tegenfeldt, B. Mehlig, M. A. Lomholt, F. Westerlund, and T. Ambjörnsson, *J. Chem. Phys.* **149**, 215101 (2018).
- [25] J. M. Polson, *Macromolecules* **51**, 5962 (2018).
- [26] D. Ödman, E. Werner, K. D. Dorfman, C. Doering, and B. Mehlig, *Biomicrofluidics* **12**, 034115 (2018).
- [27] T. Odijk, *Macromolecules* **16**, 1340 (1983).
- [28] Y. Yang, T. W. Burkhardt, and G. Gompper, *Phys. Rev. E* **76**, 011804 (2007).
- [29] T. W. Burkhardt, Y. Yang, and G. Gompper, *Phys. Rev. E* **82**, 041801 (2010).
- [30] A. V. Dobrynin, *Macromolecules* **38**, 9304 (2005).
- [31] D. Stigter, *J. Colloid Interface Sci.* **53**, 296 (1975).
- [32] D. Stigter, *Biopolymers* **16**, 1435 (1977).
- [33] Y. Wang, D. R. Tree, and K. D. Dorfman, *Macromolecules* **44**, 6594 (2011).
- [34] A. B. Bhandari, J. G. Reifenberger, H.-M. Chuang, H. Cao, and K. D. Dorfman, *J. Chem. Phys.* **149**, 104901 (2018).
- [35] D. Gupta, A. B. Bhandari, and K. D. Dorfman, *Macromolecules* **51**, 1748 (2018).
- [36] W. Reisner, K. J. Morton, R. Riehn, Y. M. Wang, Z. Yu, M. Rosen, J. C. Sturm, S. Y. Chou, E. Frey, and R. H. Austin, *Phys. Rev. Lett.* **94**, 196101 (2005).
- [37] W. Reisner, J. P. Beech, N. B. Larsen, H. Flyvbjerg, A. Kristensen, and J. O. Tegenfeldt, *Phys. Rev. Lett.* **99**, 058302 (2007).
- [38] L. H. Thamdrup, A. Klukowska, and A. Kristensen, *Nanotechnology* **19**, 125301 (2008).
- [39] P. Utko, F. Persson, A. Kristensen, and N. B. Larsen, *Lab Chip* **11**, 303 (2011).
- [40] J. A. van Kan, C. Zhang, P. Perumal Malar, and J. R. van der Maarel, *Biomicrofluidics* **6**, 036502 (2012).
- [41] E. Werner, F. Persson, F. Westerlund, J. O. Tegenfeldt, and B. Mehlig, *Phys. Rev. E* **86**, 041802 (2012).
- [42] W. F. Reinhart, J. G. Reifenberger, D. Gupta, A. Muralidhar, J. Sheats, H. Cao, and K. D. Dorfman, *J. Chem. Phys.* **142**, 064902 (2015).
- [43] H.-M. Chuang, J. G. Reifenberger, H. Cao, and K. D. Dorfman, *Phys. Rev. Lett.* **119**, 227802 (2017).
- [44] Y. Kim, K. S. Kim, K. L. Kounovsky, R. Chang, G. Y. Jung, J. J. de Pablo, K. Jo, and D. C. Schwartz, *Lab Chip* **11**, 1721 (2011).
- [45] D. R. Tree, A. Muralidhar, P. S. Doyle, and K. D. Dorfman, *Macromolecules* **46**, 8369 (2013).
- [46] A. B. Bhandari and K. D. Dorfman, *Biomicrofluidics* **13**, 044110 (2019).
- [47] H.-M. Chuang, J. G. Reifenberger, A. B. Bhandari, and K. D. Dorfman, *J. Chem. Phys.* **151**, 114903 (2019).
- [48] S. Lee, Y. Lee, Y. Kim, C. Wang, J. Park, G. Jung, Y. Chen, R. Chang, S. Ikeda, H. Sugiyama, and K. Jo, *Polymers* **11**, 15 (2019).
- [49] See Supplemental Material at <http://link.aps.org/supplemental/10.1103/PhysRevE.101.012501> for tabulated experimental parameters and details of error analysis.
- [50] T. Odijk, *J. Chem. Phys.* **125**, 204904 (2006).
- [51] J. Z. Y. Chen, *Phys. Rev. Lett.* **118**, 247802 (2017).
- [52] P. Debye and E. Hückel, *Phys. Z* **24**, 305 (1923).
- [53] S. H. Behrens and D. G. Grier, *J. Chem. Phys.* **115**, 6716 (2001).
- [54] D. Andelman, *Soft Condensed Matter Physics in Molecular and Cell Biology* (Taylor & Francis, New York, 2006).
- [55] C. Gray and P. Stiles, *Eur. J. Phys.* **39**, 053002 (2018).
- [56] B. J. Kirby and E. F. Hasselbrink, Jr., *Electrophoresis* **25**, 203 (2004).

- [57] G. K. Cheong, X. Li, and K. D. Dorfman, *Phys. Rev. E* **95**, 022501 (2017).
- [58] S. Stern, V. Shah, and B. Hardy, *J. Polym. Sci. B: Polym. Phys.* **25**, 1263 (1987).
- [59] V. Shah, B. Hardy, and S. Stern, *J. Polym. Sci. B: Polym. Phys.* **31**, 313 (1993).
- [60] K. Berean, J. Z. Ou, M. Nour, K. Latham, C. McSweeney, D. Paull, A. Halim, S. Kentish, C. M. Doherty, A. J. Hill, and K. Kalantar-zadeh, *Sep. Purif. Technol.* **122**, 96 (2014).
- [61] A. Persat, R. D. Chambers, and J. G. Santiago, *Lab Chip* **9**, 2437 (2009).